PHYSICAL REVIEW B VOLUME 45, NUMBER 16 15 APRIL 1992-II

Charge-density-wave modifications in $NbSe_3$ produced by Fe and Co doping

Zhenxi Dai, C. G. Slough, and R. V. Coleman
Physics Department, University of Virginia, Charlottesville, Virginia 22901
(Received 24 January 1992)

Dilute concentrations of impurities in $NbSe_3$ crystals change the charge-density-wave (CDW) energy gaps very rapidly while the onset temperatures show very small changes. Fe concentrations of $< 1\%$ reduce the two CDW energy gaps by approximately 30% while Co concentrations of $< 3\%$ increase the low-temperature CDW energy gap by approximately 37% and the high-temperature CDW gap by approximately 28%. The real-space scanning-tunneling-microscope scans show changes in the relative CDW modulation amplitudes consistent with the observed changes in the energy gaps.

We have used a scanning tunneling microscope (STM) operating at 4.2 K to image the surface structure of charge-density waves (CDW's) in pure $NbSe_3$ and in $NbSe_3$ doped with Fe and Co impurities. In addition, we have measured the corresponding energy-gap structure appearing in the dI/dV vs V curves at 4.2 K. The addition of dilute impurities to $NbSe_3$ does not disorder the CDW structure, but does produce very large shifts in the energy gaps associated with both the high-temperature (144 K) and the low-temperature (59 K) CDW's. The energy gaps can be shifted by 28–37% and the magnitude of the structure associated with the density-of-states (DOS) change at the gap edge can be substantially changed. Changes in CDW amplitude modulation are also observed in the real-space STM images and show a direct correlation with the energy-gap measurements.

As previously shown[1,2] for pure $NbSe_3$, the STM, which measures the local density of states (LDOS) at the Fermi level at the position of tip, detects a substantial CDW modulation on all three chains of the unit cell in the **b**-**c** plane. This result is also confirmed for the $NbSe_3$ crystals doped with Fe and Co, although the relative CDW amplitudes on the separate chains show significant changes. The three pairs of chains in $NbSe_3$ are electronically and structurally inequivalent and are denoted by I,I', II,II', and III,III' in the band-structure calculation by Shima and Kamimura.[3] The CDW with onset at 144 K is associated with the pair of chains denoted by III,III' and has wavelength[4] components of $(0.0a_0, 4.115b_0, 0.0c_0)$. The CDW with its onset at 59 K has been previously assigned[5] to the chain pair I,I' and has wavelength components of $(2.00a_0, 3.802b_0, 2.00c_0)$. $NbSe_3$ has a monoclinic unit cell. A cross section perpendicular to the chain axis (**b** axis) with the chain identifications is shown in Fig. 1. Chains II,II' were conjectured by Wilson[5] to have little or no conduction electron density and were thought not to be involved in the CDW transition.

The previous STM results[1] on pure $NbSe_3$, and the STM results reported in this paper, detect a substantial conduction electron density over chain II as well as a strong CDW modulation at the wavelength of the low-temperature CDW. Recent NMR data[6] also show a substantial conduction electron density on chains II,II', although the NMR results are not conclusive with the involvement of chains II,II' in the formation of the low-temperature CDW.

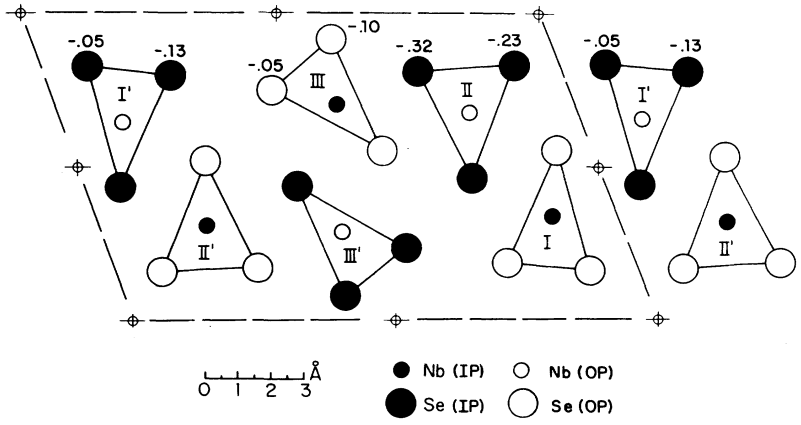

FIG. 1. Cross section of a $NbSe_3$ unit cell perpendicular to the chain axis (**b** axis). The solid atoms lie in the plane of the figure and the open atoms are out of the plane. At the **b**-**c** plane surface there are three chains per unit cell; two are in phase along the **b** axis and one is displaced by $b_0/2$ from the two in-phase chains. The height variation of the surface Se atoms is 1.52 Å. The numbers indicate the calculated negative charges of the Se atoms in the non-CDW phase. The chain designations as type I,I', II,II', and III,III' follow the nomenclature used in Ref. 3.

The measurements[1,2] from I vs V and dI/dV vs V curves on pure $NbSe_3$ with the STM have indicated CDW energy gaps of $\Delta_1 = 35.0 \pm 1.3$ meV and $\Delta_2 = 101.2 \pm 1.8$ meV for the low- and high-temperature CDW's, respectively. These values are in reasonably good agreement with previous measurements[7,8] using fixed tunnel junctions. Figure 2 shows dI/dV vs V curves measured for pure $NbSe_3$, for $Fe_{0.01}NbSe_3$, and for $Co_{0.03}NbSe_3$ single crystals, respectively. The structures labeled as $2\Delta_1$ and $2\Delta_2$ are reproducible on each type of crystal with respect to both the bias voltage and the magnitude of the conductance change observed. The $NbSe_3$ crystals doped with dilute Fe and Co show significant changes in both the magnitude and bias-voltage locations of the gap structures in the conductance curves relative to those observed for pure $NbSe_3$. For $Fe_{0.01}NbSe_3$ the average gap values calculated from seven separate conductance curves are $\Delta_1 = 24.9 \pm 1.8$ meV and $\Delta_2 = 73.2 \pm 1.1$ meV, which is an approximate 30% reduction from the values obtained for pure $NbSe_3$. The relative magnitudes of the conductance peaks observed for the two CDW gaps have also been reversed relative to pure $NbSe_3$ resulting in a significantly larger conductance peak associated with the energy gap due to the high-temperature CDW on chains III,III′ as compared with pure $NbSe_3$.

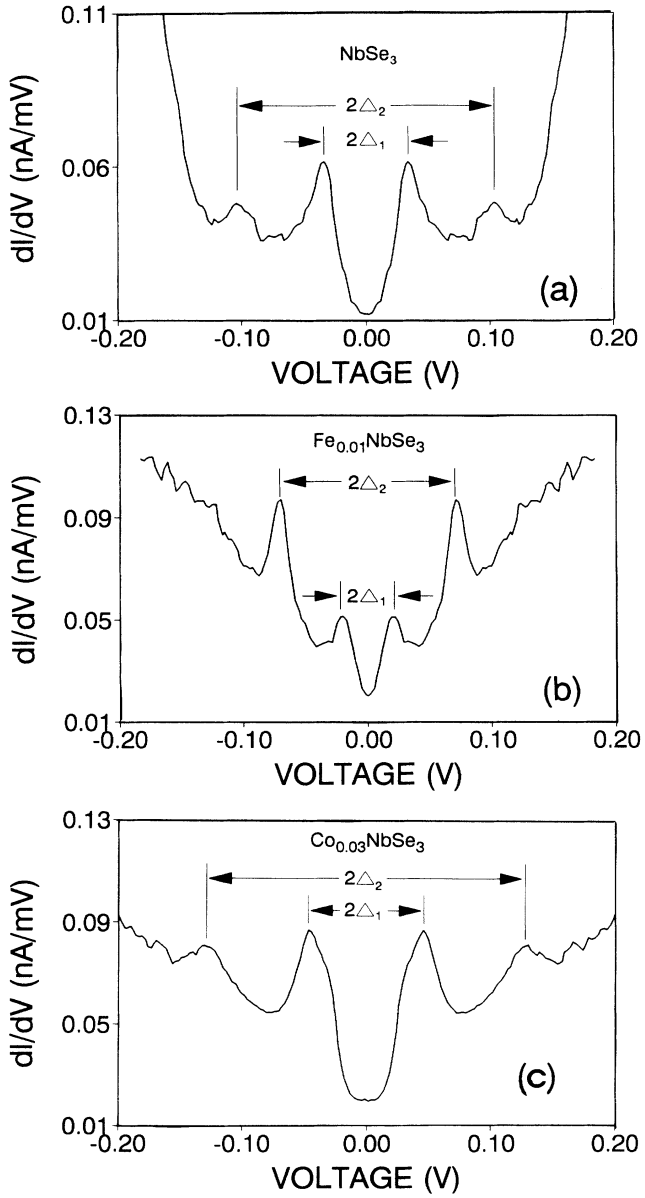

FIG. 2. Conductance vs bias-voltage curves measured at 4.2 K. The arrows indicated the gap edges for the high- and low-temperature CDW's. (a) Pure $NbSe_3$. (b) $Fe_{0.01}NbSe_3$. The relative magnitude of the high- and low-temperature CDW conductance peaks are reversed as compared with the pure material. This is consistent with the change in relative CDW amplitudes observed in the STM scans of Figs. 3 and 4. (c) $Co_{0.03}NbSe_3$. The magnitude of the low-temperature CDW conductance peaks are very strong while the high-temperature CDW conductance peaks are weak. This is also consistent with the relative CDW intensities in the STM scans of Fig. 5.

The real-space STM scans of $Fe_{0.01}NbSe_3$ show that the CDW modulation amplitude of the LDOS on chain III has also been enhanced relative to those observed on chains I′ and II as can be seen in the STM scan of Fig. 3. CDW amplitude modulation profiles of $Fe_{0.01}NbSe_3$, as obtained from Fig. 3, are shown in Fig. 4 for chains I′ and III. These confirm the larger amplitude on chain III as well as the correct identification of chain III which has the longer CDW wavelength. These relative CDW intensities and profiles can be compared to similar data on pure $NbSe_3$ contained in Ref. 1.

In contrast to the effects of Fe doping on the CDW energy gaps in $NbSe_3$, dilute Co doping produces an increase of 28–37% in the observed CDW energy gaps as shown in the conductance curve of Fig. 2(c). The resulting CDW energy-gap values for $Co_{0.03}NbSe_3$ are $\Delta_1 = 47.8 \pm 3.4$ meV and $\Delta_2 = 129.9 \pm 2.0$ meV as determined from the average of ten separate conductance curves.

The real-space STM scans also show a change in rela-

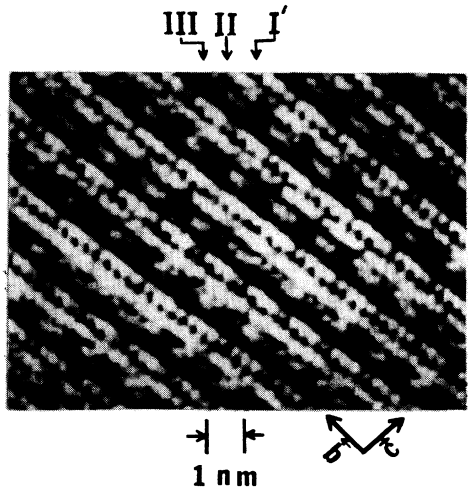

FIG. 3. Gray scale image of an STM scan on $Fe_{0.01}NbSe_3$ recorded at 4.2 K. ($I = 2$ nA, $V = 50$ mV). The image indicates that both the CDW modulation and LDOS on chain III have been increased relative to those observed on chains I′ and II when compared to pure $NbSe_3$ (see Ref. 1).

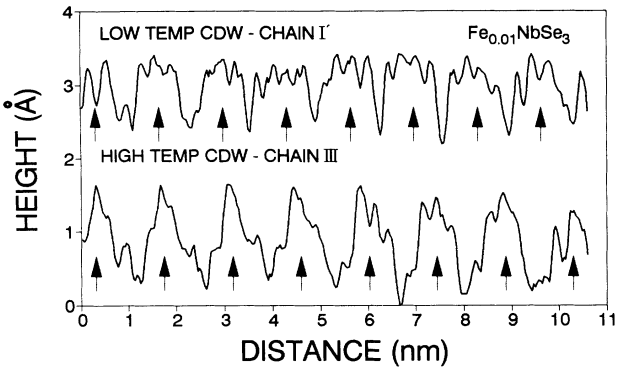

FIG. 4. Profiles of z deflection for the CDW modulation on chains I' and III for $Fe_{0.01}NbSe_3$. The profiles indicate that chain III has a larger CDW modulation amplitude than that on chain I', consistent with the spectroscopy results. The profiles also show the correct wavelength relation between the high-temperature CDW on chain III and low-temperature CDW on chain I', thereby confirming the chain assignments.

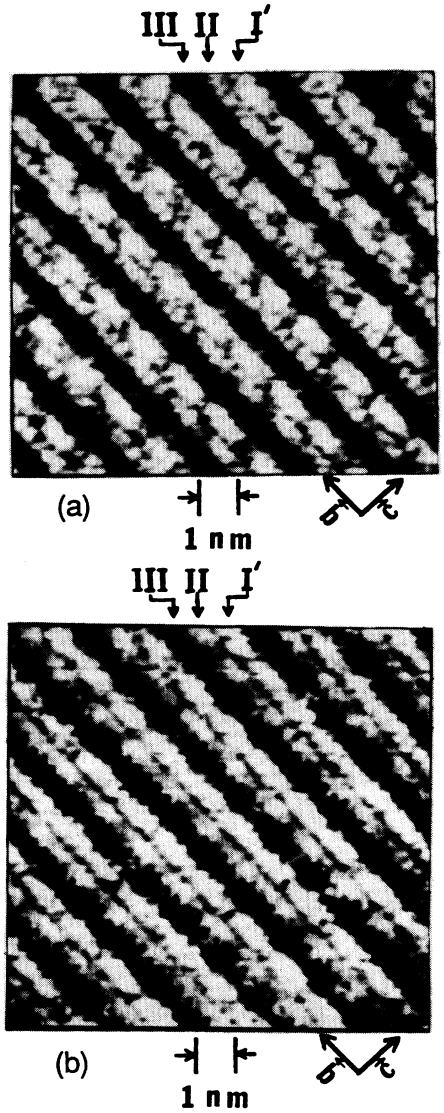

FIG. 5. Gray scale images of STM scans on $Co_{0.03}NbSe_3$ recorded at 4.2 K. The images indicate that the CDW modulation and LDOS on chain III have been depressed relative to those on chains I' and II when compared to STM images of pure $NbSe_3$ (see Ref. 1). (a) $I=2$ nA, $V=15$ mV. (b) $I=2$ nA, $V=15$ mV.

tive CDW amplitudes on the three chain types as compared with pure $NbSe_3$. As indicated in the STM scans in Fig. 5(a) and 5(b), the CDW amplitude on chain III is depressed, while chains I' and II show very strong CDW modulations at the wavelength of the low-temperature CDW. The CDW modulation on chain III is extremely weak and is barely detectable within the dark striped regions of the scan in Fig. 5(b).

The relatively weak CDW modulation on chain III is also consistent with the small magnitude of the conductance change observed at Δ_2 in the conductance curve of Fig. 2(c). The magnitude of the conductance change associated with Δ_1 is much larger, and is therefore consistent with the dominant CDW modulation on chains I' and II as observed in the STM scans of Fig. 5.

These results show that the CDW energy gaps and related Fermi-surface nesting are extremely sensitive to very dilute metal impurities. The concentrations of Fe and Co indicated are those in the starting powder from which the crystals were grown. Secondary-ion emission studies[9] on the Fe-doped crystals have shown that the final concentrations of Fe are an order of magnitude less, while at higher starting concentrations of Fe (≥ 0.10) the crystal structure changes to a different chain structure[10] which incorporates large amounts of Fe in one of the chains. Co at high concentrations does not induce a crystal phase change and is not incorporated into the chain structure in the same way. At very dilute concentrations the two impurities act in subtly different ways on the CDW structure with essentially opposite effects on the CDW energy gaps and on the relative amplitudes of the two CDW's on the different chains.

Both Fe and Co impurities increase the pinning of the CDW and induce a more complex pattern of magnetoquantum oscillation frequencies as compared to pure $NbSe_3$.[9] The magnetoquantum oscillations are due to magnetic breakdown (MB) of the CDW gaps, and the changes in frequency distributions have been explained[9] in the terms of local changes in the CDW energy gaps associated with pinning configurations of the CDW. The Co-doped crystals show a lower range of frequencies than observed in the Fe-doped crystals consistent with a larger average CDW energy gap as the present STM data indicate. Larger CDW energy gaps will reduce the size of the remaining normal Fermi-surface pockets and the external areas controlling the quantum oscillation frequencies. However, a detailed correlation of the two experiments will require considerably more data.

The energy-gap shifts of 28–37% for dilute Fe and Co doping deduced from the conductance data are not accompanied by any large shifts in the T_c for the CDW transitions. Temperature-dependence data indicate the maximum shifts to be on the order of approximately 2 K. The absence of a strong dependence of the T_c's on either

Δ_1 or Δ_2 cannot be readily explained. The values of $2\Delta_1/k_BT_1$ are 13.75, 9.78, and 18.80, and the values of $2\Delta_2/k_BT_2$ are 16.31, 11.80, and 20.94 for pure, Fe-doped and Co-doped $NbSe_3$, respectively. These values indicate very strong coupling and the mean-field relations between Δ and T_c may not hold.

Dilute impurities which induce larger changes in the T_c's also produce very large shifts in the measured energy gaps. For example, $Gd_{0.01}NbSe_3$ shows a reduction of T_1 to 53 K and T_2 to 140 K while showing a very large reduction of the high-temperature CDW energy gap to $\Delta_2 = 60.1 \pm 6.6$ meV based on an average of 19 separate conductance curves. A typical conductance versus voltage curve is shown in Fig. 6 and indicates a strong gap structure centered near approximately 60 mV while the DOS falls very rapidly at lower voltages. Structure due to the low-temperature CDW gap cannot be detected. The resistance versus temperature curves show a strong resistance anomaly associated with the high-temperature CDW, but the low-temperature CDW anomaly is strongly modified with no resistance maximum occurring below the onset at 53 K. The quantum oscillations due to MB of the low-temperature CDW gap are also quenched and cannot be detected in magnetic fields up to 230 kG. These results suggest that dilute impurities which produce larger changes in the CDW T_c's than Fe and Co are accompanied by even larger changes in the CDW energy gaps. In all cases the energy gaps are perturbed much more rapidly than the T_c's.

The CDW energy gaps may exhibit substantial anisotropy and the tunneling experiments are so far limited only to tunneling in the direction perpendicular to the b-c plane. The magnetoquantum oscillations show a frequency distribution which requires a spatial variation of the CDW energy gaps due to inhomogeneous impurity pinning of the CDW. This variation produces a strong beat structure in the oscillations arising from the MB interference network in which the fundamental frequency is controlled by a single small hole or electron pocket. The STM tunneling experiments measure an average energy gap which is not observed to vary for conductance curves taken at different points on the crystal. The large changes in this average energy gap due to the doping of $NbSe_3$ with Fe and Co may be related to the details of the pinned CDW structure and the dependence of the pinning potential on the type of impurity and its exact location in the lattice. The experimental results reported here demonstrate the extreme sensitivity of the detailed CDW amplitude structure and energy gaps to dilute impurity doping and the ability of the STM to detect these changes.

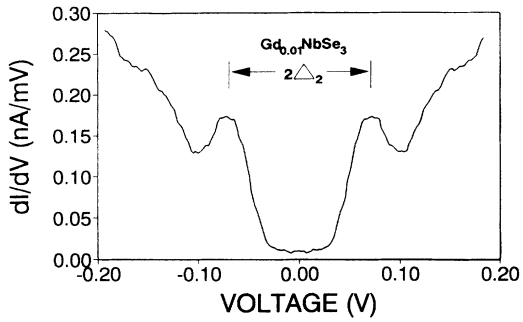

FIG. 6. Conductance vs bias-voltage curve for $Gd_{0.01}NbSe_3$ measured at 4.2 K. The arrows indicate the gap edges for the high-temperature CDW located at approximately 60 mV. The DOS within the gap region is extremely low and no structure identifiable with the low-temperature CDW gap can be detected.

This work has been supported by the U.S. Department of Energy, Grant No. DE-FG05-91ER45072. Useful discussions have been held with L. M. Falicov, V. Celli, and P. K. Hansma.

[1]Zhenxi Dai, C. G. Slough, and R. V. Coleman, Phys. Rev. Lett. **66**, 1318 (1991).

[2]R. V. Coleman, Zhenxi Dai, W. W. McNairy, C. G. Slough, and Chen Wang (unpublished).

[3]N. Shima and H. Kamimura, in *Theoretical Aspects of Band Structures and Electronic Properties of Pseudo-One-Dimensional Solids,* edited by H. Kamimura (Reidel, Boston, 1985), pp. 231–274.

[4]R. M. Fleming, D. E. Moncton, and D. W. McWhan, Phys. Rev. B **18**, 5560 (1978).

[5]J. A. Wilson, Phys. Rev. B **19**, 6456 (1979).

[6]Jianhui Shi and Joseph H. Ross, Jr. (unpublished).

[7]A. Fournel, J. P. Sorbier, M. Konczykowski, and P. Monceau, Phys. Rev. Lett. **57**, 2199 (1986).

[8]T. Ekino and J. Akimitsu, Jpn. J. Appl. Phys. **26**, 625 (1987).

[9]R. V. Coleman, M. P. Everson, Hao-An Lu, A. Johnson, and L. M. Falicov, Phys. Rev. B **41**, 460 (1990).

[10]R. J. Cava, V. L. Himes, A. D. Mighell, and R. S. Roth, Phys. Rev. B **24**, 3634 (1981).

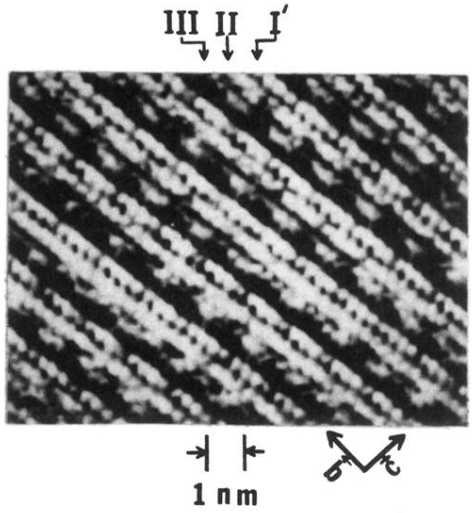

FIG. 3. Gray scale image of an STM scan on $Fe_{0.01}NbSe_3$ recorded at 4.2 K. ($I=2$ nA, $V=50$ mV). The image indicates that both the CDW modulation and LDOS on chain III have been increased relative to those observed on chains I′ and II when compared to pure $NbSe_3$ (see Ref. 1).

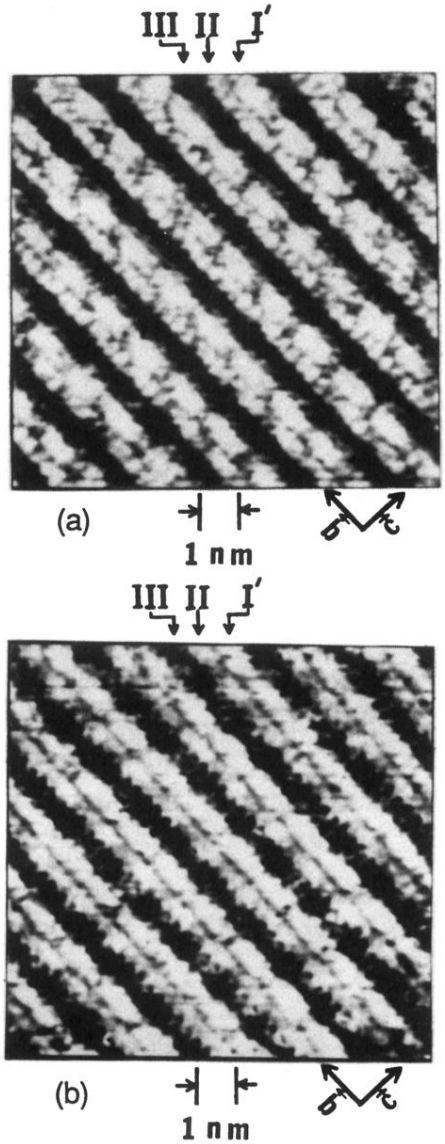

FIG. 5. Gray scale images of STM scans on $Co_{0.03}NbSe_3$ recorded at 4.2 K. The images indicate that the CDW modulation and LDOS on chain III have been depressed relative to those on chains I′ and II when compared to STM images of pure $NbSe_3$ (see Ref. 1). (a) $I=2$ nA, $V=15$ mV. (b) $I=2$ nA, $V=15$ mV.